



## RESEARCH ARTICLE

## Development of stapled NONO-associated peptides reveals unexpected cell permeability and nuclear localisation

Reginald Young<sup>1</sup>  | Tiancheng Huang<sup>1</sup> | Zijie Luo<sup>2</sup> | Yaw Sing Tan<sup>3</sup> |  
Amandeep Kaur<sup>2,4</sup> | Yu Heng Lau<sup>1,5</sup> <sup>1</sup>School of Chemistry, The University of Sydney, Camperdown, Australia<sup>2</sup>Medicinal Chemistry, Monash Institute of Pharmaceutical Sciences, Monash University, Melbourne, Australia<sup>3</sup>Bioinformatics Institute, Agency for Science, Technology and Research (A\*STAR), Matrix, Singapore<sup>4</sup>Australian Research Council Centre of Excellence for Innovations in Peptide and Protein Science, Monash University, Melbourne, Australia<sup>5</sup>Australian Research Council Centre of Excellence for Innovations in Peptide and Protein Science, The University of Sydney, Camperdown, Australia

## Correspondence

Yu Heng Lau, School of Chemistry, The University of Sydney, Eastern Ave, Camperdown, NSW 2006, Australia.

Email: [yuheng.lau@sydney.edu.au](mailto:yuheng.lau@sydney.edu.au)

## Funding information

National Health and Medical Research Council, Grant/Award Number: APP200425; Kids Cancer Alliance; Australian Research Council, Grant/Award Number: DE210101176; Australian Academy of Science

The non-POU domain-containing octamer-binding protein (NONO) is a nucleic acid-binding protein with diverse functions that has been identified as a potential cancer target in cell biology studies. Little is known about structural motifs that mediate binding to NONO apart from its ability to form homodimers, as well as heterodimers and oligomers with related homologues. We report a stapling approach to macrocyclise helical peptides derived from the insulin-like growth factor binding protein (IGFBP-3) that NONO interacts with, and also from the dimerisation domain of NONO itself. Using a range of chemistries including Pd-catalysed cross-coupling, cysteine arylation and cysteine alkylation, we successfully improved the helicity and observed modest peptide binding to the NONO dimer, although binding could not be saturated at micromolar concentrations. Unexpectedly, we observed cell permeability and preferential nuclear localisation of various dye-labelled peptides in live confocal microscopy, indicating the potential for developing peptide-based tools to study NONO in a cellular context.

## KEYWORDS

alpha helix, cell permeability, cyclic peptide, DBHS proteins, NONO, stapling

## 1 | INTRODUCTION

NONO is a member of the Drosophila behaviour/human splicing (DBHS) family of RNA-binding proteins that has a multitude of reported transcriptional regulatory roles associated with cancer proliferation.<sup>1</sup> Numerous studies have implicated NONO in tumorigenesis, with increased expression or abundance linked to malignant melanoma,<sup>2</sup> hepatocellular carcinoma,<sup>3</sup> breast cancer<sup>4</sup> and neuroblastoma.<sup>5</sup> As the molecular mechanisms driving NONO-associated

tumorigenesis are highly diverse and under active investigation,<sup>6</sup> there is significant interest in developing chemical inhibitors of NONO to interrogate its function and investigate its potential as a target for cancer therapy.

In the context of therapeutic development, NONO is a challenging target for drug discovery. Structurally, the central core of NONO dimer contains coiled-coil and NOPS domains that drive dimerisation, and two RNA recognition motif (RRM) domains that facilitate its regulatory functions.<sup>1</sup> As there are no known native small molecule binding pockets, functional disruption of NONO is likely to require inhibition of the protein-RNA or protein-protein

Reginald Young and Tiancheng Huang have equal contribution.

This is an open access article under the terms of the [Creative Commons Attribution](https://creativecommons.org/licenses/by/4.0/) License, which permits use, distribution and reproduction in any medium, provided the original work is properly cited.

© 2023 The Authors. *Journal of Peptide Science* published by European Peptide Society and John Wiley & Sons Ltd.

interaction interfaces. To date, there has only been one successful report of NONO inhibition via a covalent inhibition approach,<sup>7</sup> with no structural detail of how the inhibitor binds. Thus, peptide-based inhibitors may offer appropriate complementary modalities for expanding the chemical inhibition toolbox for interrogating NONO.<sup>8</sup>

In this study, we explored two potential native starting points for developing a stapled peptide inhibitor of NONO.<sup>9</sup> Firstly, the insulin-like growth factor binding protein 3 (IGFBP-3) has been reported to interact with NONO to regulate its function in triple-negative breast cancers.<sup>10</sup> The peptide regions from IGFBP-3 that mediate binding to NONO may therefore be amenable to chemical modification to develop an inhibitor. Secondly, mimicking the NOPS region of NONO with a modified peptide may alter its ability to function as a dynamic but obligate homodimer, heterodimer or oligomer with other members of the DBHS protein family.<sup>1,11</sup> Here, we report a comparison of different stapling methods on potential NONO-binding peptide candidates,<sup>12</sup> along with in vitro biophysical characterisation and assessment of uptake into triple-negative breast cancer cells.

## 2 | MATERIALS AND METHODS

### 2.1 | Solid-phase peptide synthesis

Fmoc solid-phase peptide synthesis was performed on Rink amide-AM polystyrene resin (0.63 mmol/g loading, 0.1 mmol, GL Biochem). Couplings were carried out by adding ethyl cyanoglyoxylate 2-oxime (4 eq, Fluorochem) to a solution of Fmoc-protected amino acid (4 eq) and *N,N'*-diisopropylcarbodiimide (4 eq) in DMF (3 mL), adding the activated amino acid solution to the resin swelled in DMF, then shaking for 1 h. Alternatively, Fmoc-protected amino acid was pre-activated with HATU (4 eq) and DIPEA (8 eq) in DMF (2 mL) for 2 min, added to the resin swelled in DMF and then incubated on shaker for 1 h. The side-chain protecting groups used were *t*-Bu for Ser, Boc for Lys/Trp, Pbf for Arg and Trt for Asn/His/Cys. Fmoc deprotection was carried out with 20% piperidine in DMF (2 × 1 min, 1 × 10 min). N-terminal capping with 5-TAMRA was carried out by pre-activating 5-TAMRA (4 eq) with HATU (4 eq) and DIPEA (8 eq) in DMF (2 mL) for 2 min, then shaking with resin swelled in DMF for 3 h. N-terminal acetyl capping was carried out with Ac<sub>2</sub>O (10 eq) and DIPEA (20 eq) in DMF (2 mL) for 1 h.

Peptides anchored on resin were cleaved in 95% TFA, 2.5% triisopropylsilane and 2.5% H<sub>2</sub>O for 2 h. For peptides containing Cys, a cleavage cocktail containing 90% TFA, 2.5% TIPS, 2.5% H<sub>2</sub>O and 5% DTT was used. After cleavage, the mixture was filtered through a polyethylene-fritted syringe and the filtrate was concentrated under a stream of nitrogen. The crude peptide was then precipitated with Et<sub>2</sub>O (2 × 10 mL) before purification by preparative HPLC.

Unless otherwise specified, all amino acid reagents were obtained from Mimotopes, and all other general reagents were obtained from Sigma Aldrich.

### 2.2 | Peptide purification and chromatographic analysis

Semi-preparative HPLC was performed on a Waters Sunfire C18 column (5 Å, 10 × 250 mm) using a Waters Prep HPLC with a 2545 quaternary pump, 2707 autosampler, 2998 PDA detector with a semi-preparative cell and WFC-III fraction collector. Peptides were eluted with a linear gradient over 30 min at a flow rate of 4 mL/min.

LCMS was performed on a Shimadzu Shim-Pack Sceptor C18-120 column (3 µm, 2.1 × 100 mm) using a Shimadzu Nexera-i LC-2040C Plus combined module system coupled to a Shimadzu LCMS-2020 mass spectrometer (ESI + single quadrupole mass detector). Peptides were typically eluted using a linear gradient of 0.1%(v/v) formic acid in Milli-Q water and 0.1%(v/v) formic acid in MeCN over 6 or 12 min at a flow rate of 0.4 mL/min. In some cases, peptides were eluted on an analytical Waters Sunfire C18 column (5 µm, 2.1 × 150 mm) over longer 30-min gradients.

Full details of all peptides synthesised and characterised in this study are provided in the [Supporting Information](#) (SI Sections 3 and 4).

### 2.3 | On-resin Pd(II)-catalysed stapling

Stapling was carried out on resin-anchored peptides synthesised up to the Fmoc-protected iodo-phenylalanine residue, based on modifications to a published procedure.<sup>13</sup> The peptide-functionalised resin (47 µmol, based on resin-loading), AgBF<sub>4</sub> (14 mg, 71 µmol, 1.5 eq), 2-nitrobenzoic acid (12 mg, 71 µmol, 1.5 eq) and Pd(OAc)<sub>2</sub> (0.5 mg, 2 µmol, 0.05 eq) were mixed in DMF (5 mL) and heated under an atmosphere of nitrogen at 90°C for 3 h. The resin was then filtered, washed with DMF (3 × 5 mL) and reacted once more to achieve greater conversion to the cyclised product. After coupling the remaining residues by Fmoc solid-phase peptide synthesis, the crude product was cleaved from the resin and purified by preparative HPLC to give the final stapled peptide.

### 2.4 | Solution-phase cysteine stapling

The procedure for perfluorobenzene (PFB) stapling was adapted from the literature.<sup>14</sup> Purified linear peptide (10 mg, 5.6 µmol) was dissolved in DMF (2.0 mL) and incubated with TCEP (1.1 eq) at rt for 30 min to reduce any disulfide bond. DIPEA (4.8 µL, 28 µmol, 5.0 eq) and perfluorobenzene (13 µL, 110 µmol, 20 eq) were added to the peptide solution, and the reaction mixture was stirred at rt for 3 h. The cyclised peptide was precipitated with Et<sub>2</sub>O (2 × 10 mL) and purified by semi-preparative HPLC.

The procedure for dibromoxylene (DBX) stapling was adapted from the literature.<sup>15,16</sup> Linear peptide (10 mg, 5.6 µmol) was dissolved in 1:1 MeCN/NH<sub>4</sub>HCO<sub>3</sub> buffer (3 mL, 50 mM, pH 8.0) and incubated with TCEP (1.1 eq) at rt for 30 min to reduce any disulfide bond. A solution of α,α'-dibromo-*m*-xylene (7.4 mg, 28 µmol, 5.0 eq) in MeCN (1 mL) was then added into the peptide solution, and the

reaction mixture was stirred at rt for 3 h. Once the reaction had reached completion or near completion, the cyclised peptide was purified by semi-preparative HPLC.

The procedure for dibromomaleimide (DBM) stapling was adapted from the literature.<sup>17</sup> Linear peptide (5 mg, 2.8  $\mu\text{mol}$ ) was dissolved in 1:1 MeCN/ $\text{NH}_4\text{HCO}_3$  buffer (1 mL, 50 mM, pH 8.0). TCEP (1.1 eq) was then added for 1 h to reduce any disulfides. 2,3-Dibromomaleimide was then added as a solution in MeCN (100 mM, 2 eq), followed by a 2-h incubation at rt. Upon completion of the reaction, the cyclised peptide was purified by semi-preparative HPLC.

## 2.5 | Circular dichroism

CD spectra were obtained on a JASCO J-1500 Circular Dichroism Spectrometer at 20°C with a 0.1 cm path length quartz cuvette, scanning from 260 to 190 nm at 20 nm/min, bandwidth 1.0 nm and response time 2 s. Each spectrum is an average of three measurements.

Purified acetyl-capped peptides were dissolved in 20% MeCN in water. The concentrations of peptides were estimated by measuring absorbance of Trp or 5-TAMRA on a Thermo NanoDrop ND-2000, using  $\epsilon = 5500 \text{ M}^{-1} \text{ cm}^{-1}$  at 280 nm and path length of 1 cm for peptides containing Trp.

Percentage helicity was calculated by taking the ratio of mean residual ellipticity at 222 nm ( $\text{MRE}_{222}$ ) over the theoretical maximum molar ellipticity at 222 nm, using the equation reported by Arora et al.,<sup>18</sup> where  $T$  is the temperature,  $k = 4$  and  $n$  is the number of amide bonds.<sup>19,20</sup>

## 2.6 | Proteolytic stability assays

Assays were run according to a previously published protocol.<sup>21</sup> TAMRA-labelled peptides were dissolved to a final concentration of 100  $\mu\text{M}$  in 100 mM Tris-HCl (pH 7.8) containing 10 mM  $\text{CaCl}_2$ , 0.3% (v/v) DMSO and 0.17% (w/w)  $\alpha$ -chymotrypsin (C4129, type II from bovine pancreas,  $\geq 40$  units/mg). The mixture was incubated at 25°C for 3 h, with 50  $\mu\text{L}$  aliquots removed at various time points. Aliquots were immediately quenched with 50  $\mu\text{L}$  MeCN, centrifuged and the supernatant analysed by analytical HPLC. Percentage of intact peptide was monitored by comparing the integration of the peptide peak against the internal standard (5-TAMRA) at 550 nm. Experiments were performed in duplicate.

## 2.7 | Recombinant NONO production

The gene encoding NONO<sub>53-312</sub> with an N-terminal His<sub>6</sub>-tag and TEV cleavage site was obtained as a synthetic gBlock (Integrated DNA Technologies), cloned into a pETDuet-1 plasmid backbone (digested with BamHI/EcoRI, New England Biolabs) by Gibson assembly and verified by Sanger sequencing. The plasmid was then transformed into BL21(DE3) *E. coli* for recombinant expression. Full gene sequences are provided in the Supporting Information (SI Section 1).

Bacteria were cultured in sterile LB (6 mL) containing ampicillin (100  $\mu\text{g}/\text{mL}$ ) at 37°C overnight. The overnight culture (1 mL) was transferred into sterile lysogeny broth (400 mL) containing ampicillin (100  $\mu\text{g}/\text{mL}$ ) and shaken at 37°C until OD<sub>600</sub> reached 0.8, then induced with IPTG at a final concentration of 0.5 mM and shaken at 18°C overnight. Cells were pelleted via centrifugation at 4°C, 3900 rcf for 30 min, then flash frozen in liquid nitrogen and stored at  $-80^\circ\text{C}$  until purification.

Cell pellets were resuspended in 20 mL binding buffer (50 mM Tris-HCl pH 7.5, 500 mM NaCl, 25 mM imidazole, 10% (v/v) glycerol) with DNase (100  $\mu\text{g}/\text{mL}$ ) and lysozyme (100  $\mu\text{g}/\text{mL}$ ) and lysed using a Bandelin Sonopuls HD 4050 with a TS-106 probe (45% amplitude, a pulse time of 4 s and interval time of 10 s for a total pulse time of 20 min, 4°C). The lysate was clarified by centrifugation at 4°C, 7197 rcf for 30 min, and the subsequent supernatant was bound onto His-Pur™ Ni-NTA resin (7 mL, Thermo Fisher Scientific). The resin was washed with 15 mL wash buffer (50 mM Tris-HCl pH 7.5, 500 mM NaCl, 50 mM imidazole, 10% (v/v) glycerol) and eluted with 10 mL elution buffer (50 mM Tris-HCl pH 7.5, 500 mM NaCl, 500 mM imidazole, 10% (v/v) glycerol). The affinity-purified protein was cleaved with His-tagged TEV protease (1:75 (w/w) TEV/NONO) at rt overnight and then purified by size-exclusion chromatography (HiLoad 16/600 Superdex 200 pg) on an ÄKTA Pure M2, eluting with running buffer (20 mM Tris-HCl pH 7.5, 250 mM NaCl, 0.5 mM EDTA, 50 mM L-proline) at a flow rate of 1 mL/min over 140 min. Fractions containing purified NONO were pooled and concentrated (SI Section 2). Protein aliquots were stored at 4°C for up to 2 weeks.

## 2.8 | Fluorescence polarisation assay

TAMRA-labelled peptide stock solutions were prepared by diluting stock solutions of peptides in DMSO (5 mM) into 20 mM Tris-HCl (pH 7.5) to a final concentration of 100 nM. Purified NONO aliquots were diluted with size-exclusion running buffer to a top concentration of 200  $\mu\text{M}$ , followed by two-fold serial dilutions to give 16-point dose-response curve.

Peptide stock (20  $\mu\text{L}$ ) and NONO dilutions (20  $\mu\text{L}$ ) were added to a 384-well fluorescence plate (Corning 3820 Assay Plate, 384-well, low volume, flat bottom, black, non-binding surface) and incubated at room temperature for 30 min. The negative control consisted of peptide stock (20  $\mu\text{L}$ ) and SEC buffer (20  $\mu\text{L}$ ) in place of the NONO dilution. Each experiment was conducted in triplicate.

Fluorescence polarisation was measured on a PHERAstar FSX Multimodal Plate Reader (BMG Labtech). Dose-response curves were fit in GraphPad Prism and dissociation constant ( $K_d$ ) was calculated via equations reported by Brown et al.<sup>22</sup>

## 2.9 | Surface plasmon resonance assay

Surface plasmon resonance was conducted on a Biacore T200 instrument (Cytiva). Biotinylated NONO was expressed recombinantly as a

His<sub>6</sub>-AviTag-NONO<sub>53-312</sub> fusion construct and purified by Ni-NTA affinity purification using the same protocols as for untagged NONO. Purified His-Avi-NONO<sub>53-312</sub> (6  $\mu$ M, 100  $\mu$ L) in size-exclusion buffer (20 mM Tris-Cl pH 7.5, 250 mM NaCl, 50 mM L-proline, 0.5 mM EDTA) was immobilised onto a CM5 sensor chip (Cytiva) coupled with streptavidin in SPR buffer at 25°C to a surface density of approximately 6000 RU. After protein immobilisation was complete, the temperature was adjusted to 6°C for protein stability and binding experiments were carried out at this temperature. Binding was tested by injecting varying concentrations of compound (2 to 200  $\mu$ M) diluted in SPR buffer containing 5%(v/v) DMSO with a contact time of 60 s, dissociation time of 120 s and flow rate of 40  $\mu$ L/min, using multiple cycle kinetics. Data were analysed on Biacore T200 Evaluation Software and fitted to a 1:1 binding model.

## 2.10 | Live cell confocal microscopy

MDA-MB-231 cells were maintained at 37°C in 5% CO<sub>2</sub>. Cells were cultured in Advanced Dulbecco's Modified Eagle's Medium (ADMEM, Thermo Fisher Scientific) supplemented with 2% foetal calf serum (FCS, Thermo Fisher Scientific) and 2.5 mM L-glutamine (Sigma-Aldrich).

For all imaging experiments, MDAMB231 cells were seeded into eight-well chamber slides (Ibidi  $\mu$ -Slide high Glass Bottom) and allowed to adhere overnight. Cells for imaging experiments had a passage number lower than 20. Images were obtained at 37°C in a 5% CO<sub>2</sub> atmosphere on a Leica SP8 Confocal Laser Scanning Microscope, equipped with an Olympus 63 $\times$  oil objective (NA 1.40) and 405, 561 and 633 nm lasers, unless otherwise stated. Images were processed using Fiji software.

All stains were purchased from Thermo Fisher Scientific. Stock solutions for MitoTracker Deep Red (M22426) were prepared in DMSO at 1 mM. NucBlue Hoechst solution in PBS (R37605) obtained from the supplier was used without dilution. The 1 mM stock solutions of the peptides were made in DMSO. For treatments, the DMSO stock was diluted into PBS supplemented with 2% FCS and then added to cells to reach a final peptide concentration of 2  $\mu$ M.

Cells were treated with 2  $\mu$ M peptide (30 min), 0.1  $\mu$ M MitoTracker Deep Red (30 min) and 2 drops/mL NucBlue Hoechst (20 min) in PBS supplemented with 2% FCS. The cells were washed twice with PBS supplemented with 2% FCS between each treatment and finally before imaging. The cells were imaged in Fluorobrite DMEM supplemented with 2% FCS.

For the blue channel (Hoechst), the cells were excited with a 405 nm laser and emission collected between 410 and 480 nm. For the green channel (TAMRA), cells were excited with a 561 nm laser and emission collected between 565 and 610 nm. For the red channel (MitoTracker), excitation was achieved using a 633 nm and emission collected between 653 and 723 nm.

Co-localisation analysis was performed using the inbuilt Coloc2 plugin in Fiji. Pearson's correlation coefficient is reported as the mean  $\pm$  SD of co-localisation analyses of five individual cells from at least two images.

## 2.11 | Molecular dynamics simulations

The structure of the IGFBP-3-derived peptide A (<sup>223</sup>HLKFLNLSPRG<sup>234</sup>) was predicted using the PEP-FOLD3<sup>23</sup> web server with default parameters (100 independent simulations and the sOPEP energy value for ranking the clusters). The second-ranked model was selected as the initial structure for molecular dynamics (MD) simulations because unlike in the first-ranked model, it does not have the unstructured C-terminal region folding onto the N-terminal helix, which could interfere with the modelling of the staple. The N- and C-termini of the peptide were capped with acetyl and N-methyl groups, respectively. Peptide Ac-A1 was generated by mutating residue 230 in peptide A to Trp and modelling the Phe-Trp staple between Phe226 and Trp230 in PyMOL.<sup>24</sup> Each of the peptides was then solvated with TIP3P<sup>25</sup> water molecules in a periodic truncated octahedron box, such that the solvent box walls are at least 15 Å away from the peptide, followed by charge neutralisation with chloride ions.

For each peptide, four independent MD simulations using different initial atomic velocities were carried out. Energy minimisations and MD simulations were performed by the PMEMD module of AMBER 18,<sup>26</sup> using the ff14SB<sup>27</sup> force field for the peptide residues and the generalised AMBER force field for the stapled residues. Atomic charges for the stapled residues were derived using the R.E.D. Server,<sup>28</sup> by fitting restrained electrostatic potential (RESP) charges<sup>29</sup> to a molecular electrostatic potential (MEP) computed by the Gaussian 09 program<sup>30</sup> at the HF/6-31G\* level of theory. All bonds involving hydrogen atoms were constrained by the SHAKE algorithm,<sup>31</sup> allowing for a time step of 2 fs. Nonbonded interactions were truncated at 9 Å, whereas long-range electrostatic interactions were accounted for by the particle mesh Ewald method<sup>32</sup> under periodic boundary conditions. Each system underwent 500 cycles of steepest-descent energy minimisation, followed by 500 cycles of conjugate-gradient energy minimisation. The system was then gradually heated to 300 K over 50 ps at constant volume before equilibration at a constant pressure of 1 atm for another 50 ps. Harmonic positional restraints with a force constant of 2.0 kcal mol<sup>-1</sup> Å<sup>-2</sup> were placed on the non-hydrogen atoms of the peptide during these energy minimisation and equilibration steps. Subsequent unrestrained equilibration (2 ns) and production (200 ns) runs were carried out at 300 K and 1 atm, using a Langevin thermostat<sup>33</sup> to maintain the temperature and a Berendsen barostat<sup>34</sup> to maintain the pressure.

## 3 | RESULTS AND DISCUSSION

### 3.1 | Pd-catalysed stapling of peptides derived from IGFBP-3

Stapling studies began with an exploration of a 12-mer peptide A (<sup>223</sup>HLKFLNLSPRG<sup>234</sup>) from IGFBP-3, which was postulated to mediate the binding to NONO reported by Baxter and co-workers.<sup>10</sup>



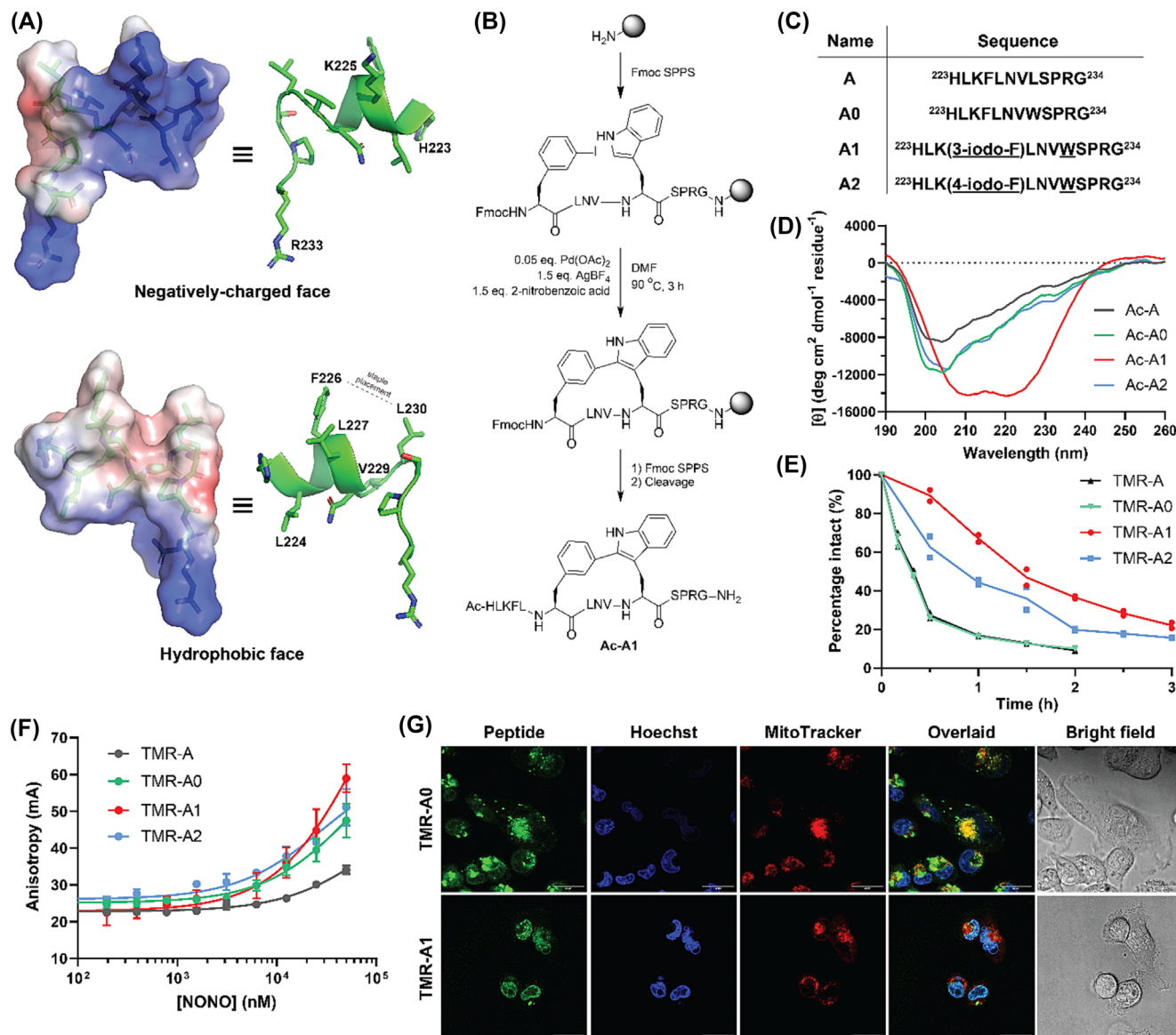


**FIGURE 1** Synthesis and evaluation of Phe-Trp-stapled IGFBP-3 peptides. (a) Predicted amphipathic helix formed by peptide **A** from IGFBP-3 based on a homology model. (b) Reaction scheme for on-resin Pd-catalysed stapling between 3-iodophenylalanine and tryptophan to produce stapled peptide **Ac-A1**. Standard Fmoc-SPPS protecting groups are used for all non-stapled residues. (c) Amino acid sequences for linear **A** and **A0** and stapled **A1** and **A2**. Peptides are C-terminally amidated and N-terminally capped with either Ac or TMR. (d) Circular dichroism spectra indicate improved helicity upon stapling with 3-iodophenylalanine in **Ac-A1** (50% helicity), whereas the 4-iodo variant **Ac-A2** and linear peptides **A0** and **A1** are less helical (<20% helicity). (e) Stapling increases stability against chymotrypsin digestion as monitored by HPLC. Helical stapled peptide **TMR-A2** shows the greatest stability, whereas the less helical stapled peptide **TMR-A1** shows moderate stability. Both linear peptides are rapidly digested. (f) Direct fluorescence polarisation assay suggests weak binding of all peptides to NONO in the micromolar range. (g) Live confocal fluorescence microscopy of MDA-MB-231 triple negative breast cancer cells shows mitochondrial localisation of linear **TMR-A0** and nuclear localisation of stapled **TMR-A1**, after treatment for 20 min with 2 μM peptide.

Homology modelling of IGFBP-3 suggests that peptide **A** is part of an alpha helix in its native context (SI Section O). An electrostatic map of the peptide based on the predicted secondary structure revealed native amphipathicity (Figure 1a), consisting of a hydrophobic face (L224, F226, L227, V229, L230) and a cationic face (H223, K225, R233). Thus, peptide **A** was considered amenable to classical peptide stapling approaches for stabilising a helical structure, with a focus on

preserving the amphiphilic nature of the peptide to promote cell permeability.<sup>35</sup>

To retain as much of the native sequence as possible, our first stapling approach was based on a L230W mutant of peptide **A**, henceforth referred to as **A0** (<sup>223</sup>HLKFLNVWSPRG<sup>234</sup>). This mutation enabled a Pd (II)-catalysed C–C bond formation reaction between residues 226 and 230 with *i, i + 4* spacing, previously reported by

Mendive-Tapia et al. for solution phase stapling of short peptides.<sup>13</sup> F226 was incorporated during peptide synthesis as 3-iodophenylalanine for coupling to W230, thus preserving F226 after stapling and placing the hydrophobic staple at the pre-existing hydrophobic face.

We successfully developed an on-resin cyclisation strategy to synthesise the target stapled peptide (Figure 1b), after initial attempts to conduct the Pd-catalysed stapling on unprotected peptides in solution based on the published conditions were low yielding (<5% yield based on HPLC).<sup>13</sup> The low yields in solution presumably arose because of poor tolerance of reactive unprotected side-chain functional groups. Using standard side-chain protecting groups for Fmoc-SPPS on Rink amide resin, peptide **A1** was partially synthesised up to the 3-iodophenylalanine residue with an N-terminal Fmoc cap. Using a modified version of the published conditions where TFA was replaced with 2-nitrobenzoic acid to minimise any premature deprotection of side-chain protecting groups, attempted cyclisation showed no conversion to the desired cyclic product after cleavage from the resin. Suspecting that the electron-withdrawing nature of the Boc protecting group on the tryptophan residue was hindering reactivity, peptide **A1** was partially resynthesised without this Boc group, after which significant conversion to the desired cyclic product was observed by LCMS analysis (60% yield by HPLC, SI Section 4). Because of the lack of tryptophan side-chain protection, we also observed some undesired reaction of the cyclic peptide with the Pbf protecting group during cleavage (SI Section 4). Nevertheless, this strategy was able to deliver a sufficient amount of the desired stapled peptide **Ac-A1** after continuation of SPPS post-cyclisation and N-terminal acetylation to complete the sequence. With this synthetic strategy in hand, the isomeric stapled analogue using 4-iodophenylalanine **Ac-A2** was also successfully synthesised (Figure 1c). In addition to these acetyl capped versions, separate batches of the peptide sequences were N-terminally capped with a 5-TAMRA dye to facilitate subsequent assays (peptides denoted by a **TMR** prefix).

The Phe-Trp staple with appropriate geometry resulted in stabilisation of an alpha-helical peptide conformation. Circular dichroism was used to assess how well matched the staple length and geometry were for the intended  $i,i + 4$  helical spacing. Stapled peptide **Ac-A1** showed a significant degree of helicity (~50% based on ellipticity at 222 nm) with clear characteristic double minima at 208 and 222 nm,<sup>36</sup> whereas stapled peptide **Ac-A2** and controls **Ac-A** and **Ac-A0** showed a low degree of helicity ( $\leq 20\%$ ) with spectra more reminiscent of a random coil structure for **Ac-A0** and **Ac-A2** (Figure 1d). Molecular dynamics simulations comparing linear **Ac-A0** and stapled **Ac-A1** show that the staple stabilises the N-terminal region in a helical conformation, whereas unfolding of the linear peptide helix was observed towards the end of the trajectories (SI Section 6). This result demonstrates the importance of staple geometry, with the C-C bond formation at the 3-position rather than the 4-position critical to achieving the desired helicity.

Proteolytic stability was increased upon stapling, correlating to the degree of peptide helicity. Stability was assessed by monitoring

peptide digestion with chymotrypsin by HPLC (Figure 1e). Both stapled peptides **TMR-A1** and **TMR-A2** underwent slower degradation than the linear controls **TMR-A** and **TMR-A0**, with **TMR-A1** showing slower degradation than **TMR-A2**, suggesting that the superior helix stabilisation for **TMR-A1** also results in superior proteolytic stability.

Binding to the target NONO protein was assessed in a direct fluorescence polarisation (FP) assay using recombinantly produced NONO<sub>53-312</sub>.<sup>11</sup> Weak binding was observed for the wild-type **TMR-A** control, with changes in anisotropy only observed above 10  $\mu\text{M}$  NONO that could not reach saturation at the maximum assay concentration of 100  $\mu\text{M}$  NONO (Figure 1f). Similar FP curves were obtained for control **TMR-A0** and stapled peptides **TMR-A1** and **TMR-A2**. These weak binding results indicate that the parent sequence from IGFBP-3 is not a potent binder of NONO and that the Pd-catalysed stapling approach was unable to improve the binding sufficiently under the conditions tested.

Although binding to NONO was poor, we observed a remarkable capacity for the peptides to rapidly enter cells. Cell uptake was qualitatively assessed by live confocal fluorescence microscopy in MDA-MB-231 cells, a triple-negative breast cancer cell line similar to those used by Baxter and co-workers when identifying the interactions between NONO and IGFBP-3 (Figure 1g).<sup>10</sup> Cells were treated with 2  $\mu\text{M}$  of **TMR-A0** or **TMR-A1** for 20 min in standard growth media (including serum), and then the cells were imaged after co-staining with Hoechst and MitoTracker dyes to assess co-localisation with the nucleus and mitochondria, respectively (SI Section 7). Linear **TMR-A0** was primarily localised to the mitochondria (Pearson's correlation coefficient,  $R = 0.64 \pm 0.04$ ), whereas stapled **TMR-A1** was primarily localised to the nucleus ( $R = 0.76 \pm 0.05$ ). This result suggests that the staple is able to redirect subcellular localisation to the nucleus where the intended target NONO primarily resides.

### 3.2 | Cysteine-stapled IGFBP-3 stapled peptides

In search of higher affinity peptides, we explored the effect of alternative cyclisation chemistries and stapling positions. We applied established cysteine stapling methods to the IGFBP-3 peptide sequence **A** in an  $i,i + 4$  format, making substitutions N228C and P232C to install the cysteines. This positioning was chosen to remove the known helix-breaking residue proline from the sequence, resulting in linear peptide sequence **B0** (<sup>223</sup>HLKFLC<sup>234</sup>VLSCRG<sup>234</sup>). After synthesising the linear precursor **TMR-B0**, in-solution stapling of unprotected peptides with perfluorobenzene (PFB) and 1,3-dibromoxylene (DBX) linkers resulted in stapled peptides **TMR-B1** and **TMR-B2**, respectively (Figure 2a).<sup>14-16</sup>

In our direct FP assay for assessing binding to NONO, binding for these B-series peptides was improved in all cases relative to the A-series, suggesting that substitutions at these positions were more well-tolerated, although binding could still not be saturated at 100  $\mu\text{M}$  (Figure 2b). Choosing **TMR-B0** and **TMR-B2** for further analysis, both were cell permeable according to fluorescence confocal microscopy on MDA-MB-231 cells (Figure 2c), with nuclear

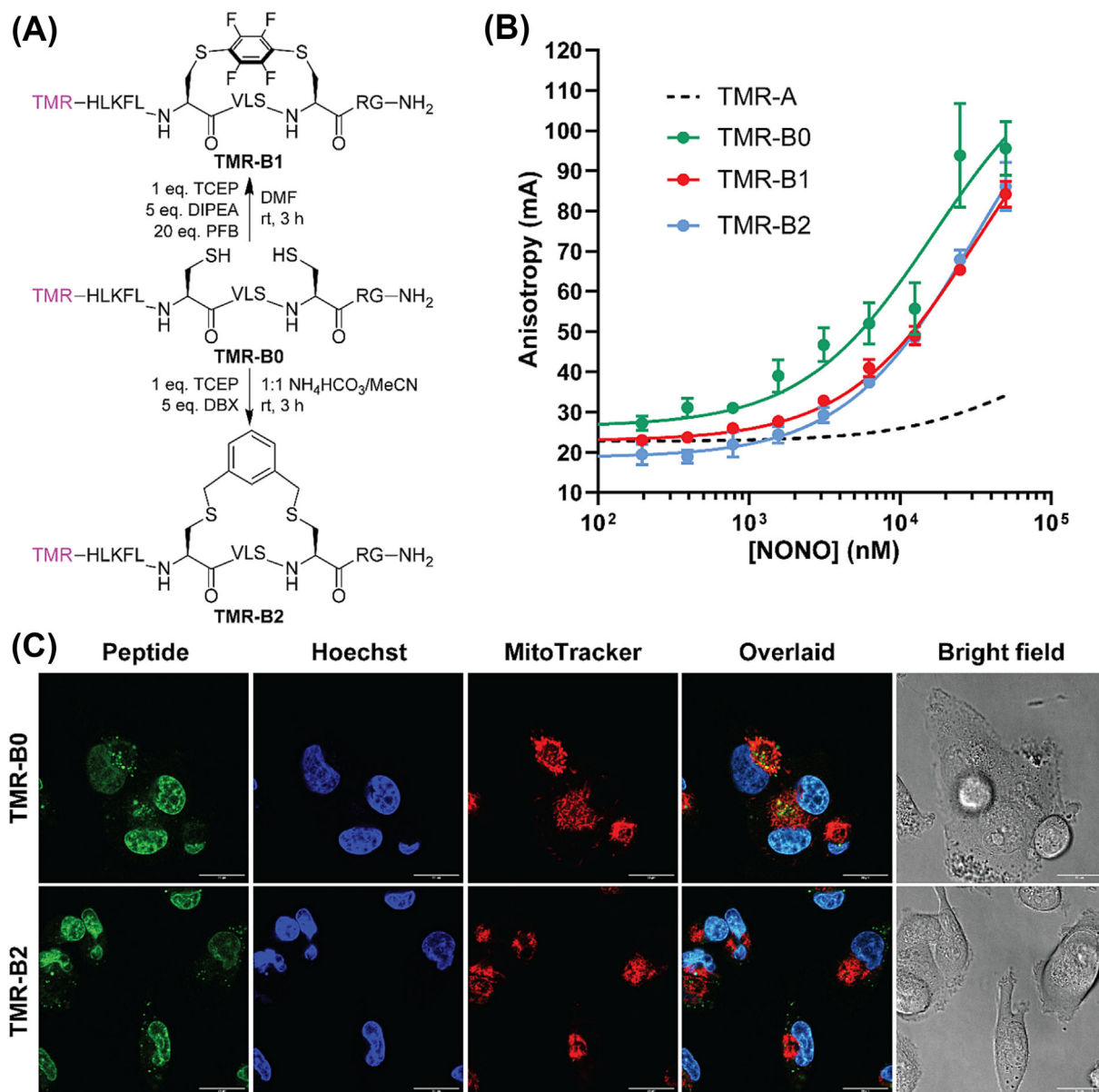


**FIGURE 2** Synthesis and evaluation of cysteine-stapled IGFBP-3 peptides. (a) Reaction scheme for cysteine stapling with perfluorobenzene and *m*-dibromoxylene to produce stapled peptides **TMR-B1** and **TMR-B2**. (b) Direct fluorescence polarisation assay suggests stronger binding of all peptides to NONO relative to the A-series of peptides in Figure 1. (c) Live confocal fluorescence microscopy of MDA-MB-231 cells shows nuclear localisation for both **TMR-B0** and **TMR-B2** after treatment for 20 min with 2  $\mu\text{M}$  peptide.

localisation seen for both linear and stapled peptides in this instance ( $R = 0.82 \pm 0.05$  and  $0.80 \pm 0.08$ , respectively).

### 3.3 | Cysteine stapling of peptides from the NONO dimerisation domain

Finally, we explored the stapling of partially helical peptides derived from the NOPS domain of NONO that facilitates its dimerisation. An initial exploration of three overlapping 15-mer peptides **C-E** from residues 250–271 of the NOPS region led to the identification of peptide sequence **C** ( $^{257}\text{FAQPGSFYEYAMRW}^{271}$ ) as the only sequence with

any appreciable signal in direct FP for measuring binding to NONO (SI Section 8). Crucially, peptide sequence **C** including residues Y267 and W271 that are thought to be the critical residues for mediating NONO homodimerisation (Figure 3a).

A double cysteine mutant sequence **C0** ( $^{256}\text{RFAQPGSFCEYACRW}^{271}$ ) was designed based on the sequence of **C**, incorporating Y265C and M269C changes with *i, i + 4* spacing on the opposite face to the critical Y267 and W271 residues, while also including an extra N-terminal residue R256 to enhance solubility. The cysteine residues were then stapled using either a DBX linker or a 2,3-dibromomaleimide (DBM) linker, giving stapled peptides **TMR-C1** and **TMR-C2**, respectively (Figure 3b).

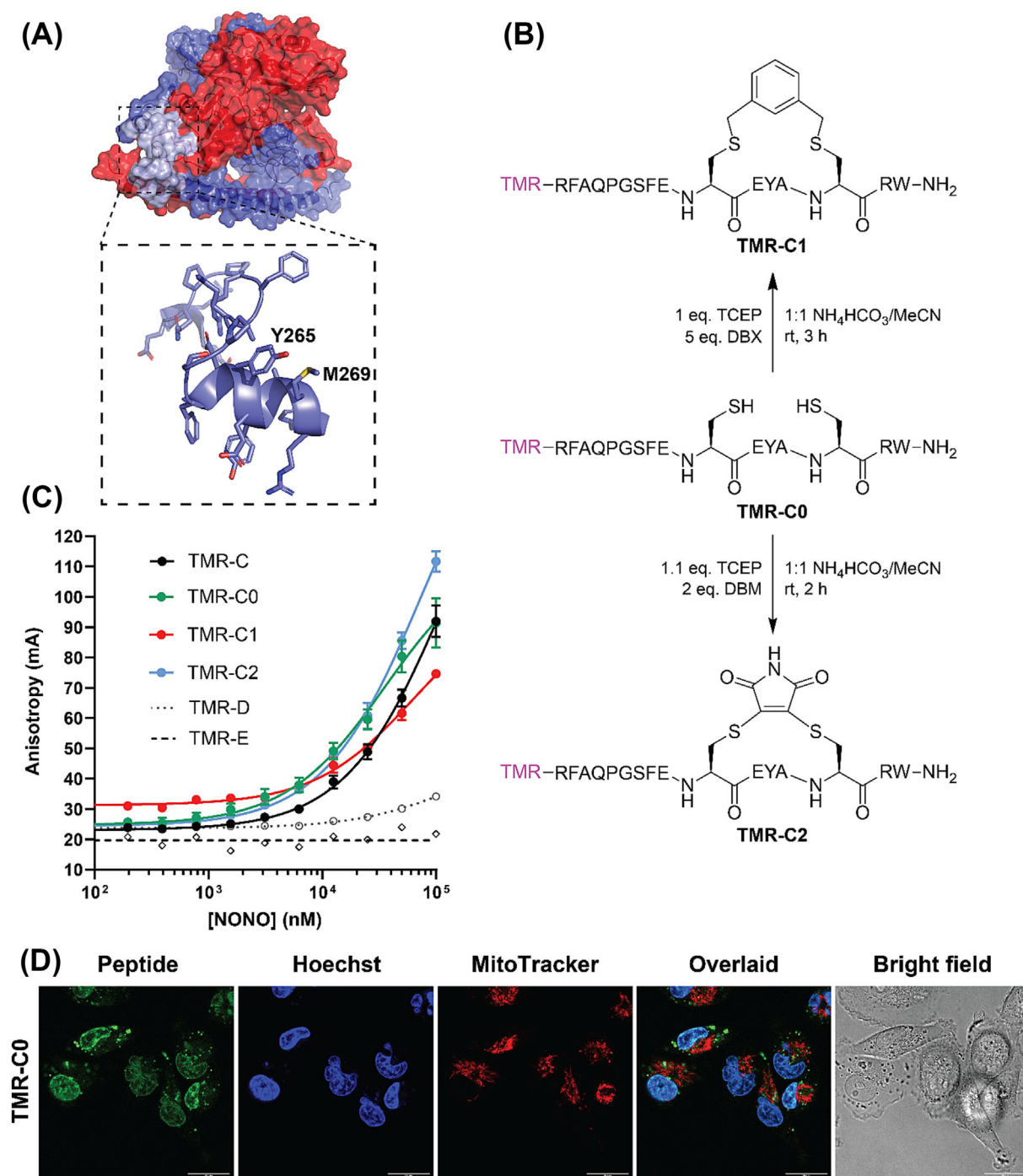


**FIGURE 3** Synthesis and evaluation of cysteine stapled NONO peptides. (a) Partially alpha-helical peptide from the NOPS region of the NONO dimer, showing the key residues Y265 and M269 that mediate NONO dimerisation. (b) Reaction scheme for cysteine stapling with *m*-dibromoxylene and dibromomaleimide to produce stapled peptides **TMR-C1** and **TMR-C2**. (c) Direct fluorescence polarisation assay suggests modest binding to NONO similar to the peptides from the B-series. Other linear NONO-derived peptides **TMR-D** and **TMR-E** showed no binding. (d) Live confocal fluorescence microscopy of MDA-MB-231 cells shows nuclear localisation for **TMR-C0** after treatment for 20 min with 2  $\mu$ M peptide, whereas **TMR-C1** was not cell permeable.

In direct FP assays, both stapled peptides **TMR-C1** and **TMR-C2** and the linear precursor **TMR-C0** all displayed modest binding to NONO, similar to that of the B-series peptides (Figure 3c), although **TMR-C1** appeared to exhibit some time-dependent loss of binding after incubating for an additional 2 h. To support the results from the

FP assay, surface plasmon resonance conducted on the non-labelled **Ac-C2** also demonstrated binding in an orthogonal assay, although again with insufficient saturation at mid-micromolar concentrations to calculate accurate affinities (SI Section 9). Testing **TMR-C0** and **TMR-C2** in MDA-MB-231 cells, linear **TMR-C0** was found to localise to the



nucleus (Figure 3d), but there was no observed intracellular fluorescence for **TMR-C2**. Unlike the behaviour of the A- and B-series peptides, this unexpected observation suggests a complex interplay between sequence and staple that controls cell permeability and sub-cellular localisation.

## 4 | CONCLUSIONS

We successfully synthesised stapled versions of putative NONO-binding peptides derived from the binding partner IGFBP-3 and the NOPS region of NONO itself, applying a variety of macrocyclisation chemistries. Pd(II)-catalysed cross-coupling of the IGFBP-3 sequence led to improved helicity and proteolytic stability but displayed only weak binding to NONO.

In our application of the Pd(II)-catalysed stapling reaction, we successfully developed on-resin cyclisation conditions to broaden the limited functional group tolerance that was observed when attempting the original solution-phase protocol.<sup>13</sup> In particular, cyclisation immediately after the iodo-phenylalanine residue and omission of side-chain Boc protection of tryptophan were important factors in achieving the desired macrocyclisation reaction.

Stapling of the IGFBP-3 and NOPS peptides by cross-linking cysteines with perfluorobenzene, dibromomaleimide or biphenyl linkers led to improved but not saturable binding to NONO. This binding behaviour may be symptomatic of the natural preference and function of the protein as a promiscuous RNA binder that is also capable of oligomerisation via coiled-coil interactions.<sup>1</sup> NONO and its DBHS paralogues have all been reported as one of the most frequently detected hits in affinity purification mass spectrometry workflows, attributed to general non-specific interactions<sup>37</sup>; hence, caution is recommended when interpreting any biological findings. Given the recent report of a successful covalent approach however, a covalent peptide inhibitor strategy may have future promise in yielding potent and selective NONO inhibitors.

Remarkably, five of the six dye-labelled peptides assessed by fluorescence microscopy showed uptake into breast cancer cell lines, four of which displaying a preference for nuclear localisation. Given that both stapled and linear peptides were observed to enter cells, this finding suggests that the sequences themselves possess inherent cell-penetrating and nuclear-localising properties, which are maintained in two of the three stapled versions. Given the DBM-stapled NOPS peptide does not enter cells and all the IGFBP-3 peptides do, the data suggest that the amphiphilic nature of IGFBP-3 and its stapled variants may be a contributing factor towards uptake. The possibility of partial decomposition or the effects of dye labelling on peptide localisation during microscopy cannot be completely eliminated,<sup>38</sup> especially for the more proteolytically vulnerable linear peptides. Nevertheless, the short 20-min window of incubation and differential behaviour between the various peptides suggests that the observed effects are likely reflective of the original intact peptides rather than general label-induced effects or decomposition.

Overall, this work has shown that stapling can improve helicity and stability in the case of peptide **A1** and induce changes in target binding and cell permeability properties, providing promise for the downstream development of more potent NONO-binding peptides that maintain favourable uptake properties, as well as potential for further investigation as cell-penetrating peptides.

## ACKNOWLEDGEMENTS

We thank Emeritus Professor Robert Baxter and Hasanthi de Silva (Kolling Institute) for preliminary assistance with cellular studies and microscopy. We also thank Professor Charlie Bond and Dr Andrew Marshall (University of Western Australia) for advice on producing recombinant NONO and Dr Lorna Wilkinson-White for assistance with surface plasmon resonance. YHL acknowledges funding from the National Health and Medical Research Council (APP200425), and TH acknowledges funding from the Kids Cancer Alliance. AK acknowledges funding from the Australian Research Council (DE210101176) and the Australian Academy of Science (JG Russell Award). Open access publishing facilitated by The University of Sydney, as part of the Wiley - The University of Sydney agreement via the Council of Australian University Librarians.

## ORCID

Reginald Young  <https://orcid.org/0009-0005-5163-7567>

Yu Heng Lau  <https://orcid.org/0000-0001-6560-8410>

## REFERENCES

- Knott GJ, Bond CS, Fox AH. The DBHS proteins SFPQ, NONO and P54Nrb: a multipurpose molecular scaffold. *Nucleic Acids Res.* 2016; 44(9):3989-4004. doi:10.1093/nar/gkw271
- Schiffner S, Zimara N, Schmid R, Bosserhoff A-K. P54 Nrb is a new regulator of progression of malignant melanoma. *Carcinogenesis.* 2011;32(8):1176-1182. doi:10.1093/carcin/bgr103
- Shen M, Zhang R, Jia W, et al. Nuclear scaffold protein P54nrb/NONO facilitates the hypoxia-enhanced progression of hepatocellular carcinoma. *Oncogene.* 2021;40(24):4167-4183. doi:10.1038/s41388-021-01848-9
- Pavao M, Huang Y-H, Hafer LJ, Moreland RB, Traish AM. Immunodetection of Nmt55/P54nrb isoforms in human breast cancer. *BMC Cancer.* 2001;1(1):15. doi:10.1186/1471-2407-1-15
- Liu PY, Erriquez D, Marshall GM, et al. Effects of a novel long noncoding RNA, IncUSMycN, on N-Myc expression and neuroblastoma progression. *J Natl Cancer Inst.* 2014;106(7). doi:10.1093/jnci/dju113
- Feng P, Li L, Deng T, et al. NONO and tumorigenesis: more than splicing. *J Cell Mol Med.* 2020;24(8):4368-4376. doi:10.1111/jcmm.15141
- Kathman SG, Koo SJ, Lindsey GL, et al. Remodeling oncogenic transcriptomes by small molecules targeting NONO. *Nat Chem Biol.* 2023; 19(7):825-836. doi:10.1038/s41589-023-01270-0
- Valeur E, Guéret SM, Adihou H, et al. New modalities for challenging targets in drug discovery. *Angew Chem Int Ed.* 2017;56(35):10294-10323. doi:10.1002/anie.201611914
- Bluntzer MTJ, O'Connell J, Baker TS, Michel J, Hulme AN. Designing stapled peptides to inhibit protein-protein interactions: an analysis of successes in a rapidly changing field. *Peptide Sci.* 2021;113(1):e24191. doi:10.1002/pep2.24191
- De Silva HC, Lin MZ, Phillips L, Martin JL, Baxter RC. IGFBP-3 interacts with NONO and SFPQ in PARP-dependent DNA damage repair in triple-negative breast cancer. *Cell Mol Life Sci.* 2019;76(10):2015-2030. doi:10.1007/s00018-019-03033-4

11. Lee M, Sadowska A, Bekere I, et al. The structure of human SFPQ reveals a coiled-coil mediated polymer essential for functional aggregation in gene regulation. *Nucleic Acids Res.* 2015;43(7):3826-3840. doi:10.1093/nar/gkv156
12. Lau YH, de Andrade P, Wu Y, Spring DR. Peptide stapling techniques based on different macrocyclisation chemistries. *Chem Soc Rev.* 2014;44(1):91-102. doi:10.1039/c4cs00246f
13. Mendive-Tapia L, Preciado S, García J, et al. New peptide architectures through C-H activation stapling between tryptophan-phenylalanine/tyrosine residues. *Nat Commun.* 2015;6(1):7160. doi:10.1038/ncomms8160
14. Spokoiny AM, Zou Y, Ling JJ, Yu H, Lin Y-S, Pentelute BL. A perfluoroaryl-cysteine S<sub>N</sub>Ar chemistry approach to unprotected peptide stapling. *J Am Chem Soc.* 2013;135(16):5946-5949. doi:10.1021/ja400119t
15. Timmerman P, Beld J, Puijk WC, Meloen RH. Rapid and quantitative cyclization of multiple peptide loops onto synthetic scaffolds for structural mimicry of protein surfaces. *ChemBioChem.* 2005;6(5):821-824. doi:10.1002/cbic.200400374
16. Jo H, Meinhardt N, Wu Y, et al. Development of  $\alpha$ -helical calpain probes by mimicking a natural protein-protein interaction. *J Am Chem Soc.* 2012;134(42):17704-17713. doi:10.1021/ja307599z
17. Grison CM, Burslem GM, Miles JA, et al. Double quick, double click reversible peptide "stapling". *Chem Sci.* 2017;8(7):5166-5171. doi:10.1039/C7SC01342F
18. Wang D, Chen K, Kulp JL, Arora PS. Evaluation of biologically relevant short  $\alpha$ -helices stabilized by a main-chain hydrogen-bond surrogate. *J Am Chem Soc.* 2006;128(28):9248-9256. doi:10.1021/ja062710w
19. Luo P, Baldwin RL. Mechanism of helix induction by trifluoroethanol: a framework for extrapolating the helix-forming properties of peptides from trifluoroethanol/water mixtures back to water. *Biochemistry.* 1997;36(27):8413-8421. doi:10.1021/bi9707133
20. Shepherd NE, Hoang HN, Abbenante G, Fairlie DP. Single turn peptide alpha helices with exceptional stability in water. *J Am Chem Soc.* 2005;127(9):2974-2983. doi:10.1021/ja0456003
21. Lau YH, Wu Y, Rossmann M, et al. Double strain-promoted macrocyclization for the rapid selection of cell-active stapled peptides. *Angew Chem Int Ed.* 2015;54(51):15410-15413. doi:10.1002/anie.201508416
22. Brown CJ, Quah ST, Jong J, et al. Stapled peptides with improved potency and specificity that activate P53. *ACS Chem Biol.* 2013;8(3):506-512. doi:10.1021/cb3005148
23. Lamiable A, Thévenet P, Rey J, Vavrusa M, Derreumaux P, Tufféry P. PEP-FOLD3: faster de novo structure prediction for linear peptides in solution and in complex. *Nucleic Acids Res.* 2016;44(W1):W449-W454. doi:10.1093/nar/gkw329
24. DeLano WL. *The PyMOL molecular graphics system*, 2002.
25. Jorgensen WL, Chandrasekhar J, Madura JD, Impey RW, Klein ML. Comparison of simple potential functions for simulating liquid water. *J Chem Phys.* 1983;79(2):926-935. doi:10.1063/1.445869
26. Case DA, Ben-Shalom IY, Brozell SR, Cerutti DS, Cheatham TE III, VWD Cruzeiro, Darden TA, Duke RE, Ghoreishi D, Gilson MK, Gohlke H, Goetz AW, Greene D, Harris R, Homeyer N, Izadi S, Kovalenko A, Kurtzman T, Lee TS, LeGrand S, Li P, Lin C, Liu J, Luchko T, Luo R, Mermelstein DJ, Merz KM, Miao Y, Monard G, Nguyen C, Nguyen H, Omelyan I, Onufriev A, Pan F, Qi R, Roe DR, Roitberg A, Sagui C, Schott-Verdugo S, Shen J, Simmerling CL, Smith J, Salomon-Ferrer R, Swails J, Walker RC, Wang J, Wei H, Wolf RM, Wu X, Xiao L, York DM, Kollman PA. *AMBER 18*, 2018.
27. Maier JA, Martinez C, Kasavajhala K, Wickstrom L, Hauser KE, Simmerling C. ff14SB: improving the accuracy of protein side chain and backbone parameters from ff99SB. *J Chem Theory Comput.* 2015;11(8):3696-3713. doi:10.1021/acs.jctc.5b00255
28. Vanquielef E, Simon S, Marquant G, et al. Server: a web service for deriving RESP and ESP charges and building force field libraries for new molecules and molecular fragments. *Nucleic Acids Res.* 2011;39(suppl\_2):W511-W517. doi:10.1093/nar/gkr288
29. Cornell WD, Cieplak P, Bayly CI, Kollman PA. Application of RESP charges to calculate conformational energies, hydrogen bond energies, and free energies of solvation. *J Am Chem Soc.* 1993;115(21):9620-9631. doi:10.1021/ja00074a030
30. Frisch M. J., Trucks G. W., Schlegel H. B., Scuseria G. E., Robb M. A., Cheeseman J. R., Scalmani G., Barone V., Petersson G. A., Nakatsuji H., Li X., Caricato M., Marenich A., Bloino J., Janesko B. G., Gomperts R., Mennucci B., Hratchian H. P., Ortiz J. V., Izmaylov A. F., Sonnenberg J. L., Williams-Young D., Ding F., Lipparini F., Egidi F., Goings J., Peng B., Petrone A., Henderson T., Ranasinghe D., Zakrzewski V. G., Gao J., Rega N., Zheng G., Liang W., Hada M., Ehara M., Toyota K., Fukuda R., Hasegawa J., Ishida M., Nakajima T., Honda Y., Kitao O., Nakai H., Vreven T., Throssell K., Montgomery, Jr. J. A., Peralta J. E., Ogliaro F., Bearpark M., Heyd J. J., Brothers E., Kudin K. N., Staroverov V. N., Keith T., Kobayashi R., Normand J., Raghavachari K., Rendell A., Burant J. C., Iyengar S. S., Tomasi J., Cossi M., Millam J. M., Klene M., Adamo C., Cammi R., Ochterski J. W., Martin R. L., Morokuma K., Farkas O., Foresman J. B., Fox D. J. *Gaussian 09, Revision B.1*, 2009.
31. Ryckaert J-P, Ciccotti G, Berendsen HJC. Numerical integration of the Cartesian equations of motion of a system with constraints: molecular dynamics of n-alkanes. *J Comput Phys.* 1977;23(3):327-341. doi:10.1016/0021-9991(77)90098-5
32. Darden T, York D, Pedersen L. Particle mesh Ewald: an N-log(N) method for Ewald sums in large systems. *J Chem Phys.* 1993;98(12):10089-10092. doi:10.1063/1.464397
33. Izaguirre JA, Catarella DP, Wozniak JM, Skeel RD. Langevin stabilization of molecular dynamics. *J Chem Phys.* 2001;114(5):2090-2098. doi:10.1063/1.1332996
34. Berendsen HJC, Postma JPM, van Gunsteren WF, DiNola A, Haak JR. Molecular dynamics with coupling to an external bath. *J Chem Phys.* 1984;81(8):3684-3690. doi:10.1063/1.448118
35. Hoang HN, Hill TA, Fairlie DP. Connecting hydrophobic surfaces in cyclic peptides increases membrane permeability. *Angew Chem Int Ed.* 2021;60(15):8385-8390. doi:10.1002/anie.202012643
36. Greenfield NJ. Using circular dichroism spectra to estimate protein secondary structure. *Nat Protoc.* 2006;1(6):2876-2890. doi:10.1038/nprot.2006.202
37. Mellacheruvu D, Wright Z, Couzens AL, et al. The CRAPome: a contaminant repository for affinity purification-mass spectrometry data. *Nat Methods.* 2013;10(8):730-736. doi:10.1038/nmeth.2557
38. Cunningham CW, Mukhopadhyay A, Lushington GH, Blagg BSJ, Prinszano TE, Krise JP. Uptake, distribution and diffusivity of reactive fluorophores in cells: implications toward target identification. *Mol Pharm.* 2010;7(4):1301-1310. doi:10.1021/mp100089k

## SUPPORTING INFORMATION

Additional supporting information can be found online in the Supporting Information section at the end of this article.

**How to cite this article:** Young R, Huang T, Luo Z, Tan YS, Kaur A, Lau YH. Development of stapled NONO-associated peptides reveals unexpected cell permeability and nuclear localisation. *J Pept Sci.* 2024;30(5):e3562. doi:10.1002/psc.3562